Activity-induced gene expression in the human brain

Snehajyoti Chatterjee[1,2#], Brian J. Park[3#], Yann Vanrobaeys[1#], Shane A. Heiney[1,2,4], Ariane E. Rhone[3], Kirill V. Nourski[3], Lucy Langmack[1,2], Utsav Mukherjee[1,2], Christopher K. Kovach[3], Zsuzsanna Kocsis[3,5], Yukiko Kikuchi[5], Christopher I. Petkov[3,5], Marco M. Hefti[6], Ethan Bahl[7], Jacob J Michaelson[7], Hiroto Kawasaki[3], Hiroyuki Oya[3], Matthew A. Howard III[3], Thomas Nickl-Jockschat[1,2,7], Li-Chun Lin[1,2,8], Ted Abel[1,2,7*]

Affiliations:

[1] Department of Neuroscience and Pharmacology, Iowa Neuroscience Institute Carver College of Medicine, University of Iowa, Iowa City, IA, USA

[2] Iowa Neuroscience Institute, University of Iowa, Iowa City, IA, USA

[3] Department of Neurosurgery, University of Iowa Hospitals and Clinics, Iowa City, IA, USA

[4] Neural Circuits and Behavior Core, Iowa Neuroscience Institute Carver College of Medicine, University of Iowa, Iowa City, IA, USA

[5] Biosciences Institute, Newcastle University Medical School, Newcastle upon Tyne, UK

[6] Department of Pathology, University of Iowa Hospitals and Clinics, Iowa City, IA, USA

[7]Department of Psychiatry, University of Iowa Hospitals and Clinics, Iowa City, IA, USA

[8]Iowa NeuroBank Core, Iowa Neuroscience Institute Carver College of Medicine, University of Iowa, Iowa City, IA, USA

[#]Authors contributed equally

*Corresponding author: ted-abel@uiowa.edu

Keywords:

Electrical stimulation, microglia, anterior temporal neocortex, single nuclei multiomics

Key findings

- Electrical stimulation of the human cortex allows the identification of an activity-dependent gene expression signature.
- Neurons and microglia in the human brain exhibit distinct transcriptional signatures following electrical stimulation.
- Single nuclear chromatin accessibility studies reveal cell-type-specific epigenomic changes and specific transcription factor motifs in microglia.

Abstract

Activity-induced gene expression underlies synaptic plasticity and brain function. Here, using molecular sequencing techniques, we define activity-dependent transcriptomic and epigenomic changes at the tissue and single-cell level in the human brain following direct electrical stimulation of the anterior temporal lobe in patients undergoing neurosurgery. Genes related to transcriptional regulation and microglia-specific cytokine activity displayed the greatest induction pattern, revealing a precise molecular signature of neuronal activation in the human brain.

47 **Main**

48 Activity-induced gene expression underlies the ability of the brain to learn and adapt to
49 environmental stimuli. Dynamic changes in transcriptomic patterns are essential for
50 cognition[1-3], affective processing[4], addiction[5], and the initiation of behaviors[6,7].
51 However, these experiments have been mostly conducted in rodents[8,9] and human
52 induced pluripotent stem cells[10], and it remains unknown how closely they reflect actual
53 processes in the living human brain. Studies of activity-dependent gene expression in
54 humans *in vivo* are lacking due to the availability and accessibility of tissue that can be
55 acutely manipulated. Direct current electrical stimulation is used in the field of epilepsy
56 surgery and could provide a major avenue to address this important challenge.
57 Stimulation of the amygdala in epileptic patients enhances declarative memory[11], and
58 closed-loop stimulation of the lateral temporal cortex rescues intervals of poor memory
59 encoding[12]. Moreover, electrical stimulation is an effective, therapeutic tool to improve
60 memory[12] and depression[13]. Here, we applied direct electrical stimulation of the
61 anterior temporal lobe of patients undergoing neurosurgery to examine activity-
62 dependent changes in gene expression and chromatin accessibility in the human brain
63 for the first time.

64

65 We recruited 8 adult neurosurgical patients undergoing surgical resection of seizure foci
66 following clinical monitoring to treat epilepsy. The patients underwent an anterior
67 temporal lobectomy, during which samples were resected from the neocortex and
68 processed immediately after removal. The participants were evenly distributed between
69 two experimental paradigms. For the first group (stimulated paradigm, n=4 subjects), a

70 sample was at baseline and then an adjacent region of cortex was stimulated using
71 bipolar electrical stimulation (50 Hz). Thirty minutes later, a sample was taken from the
72 stimulated region **(Fig. 1a; Extended Data Fig. 1, Supplementary Table 1)** In the
73 second group (unstimulated paradigm, n=4 subjects), a sample was taken at baseline
74 and then 30 min later a second sample was taken without stimulation **(Fig. 1b;**
75 **Extended Data Fig. 1)**. Tissue was subjected to whole-transcriptome RNA sequencing
76 (RNA-seq) to identify activity-induced genes following electrical stimulation. RNA-seq
77 analysis from the stimulated and baseline samples revealed 124 significantly
78 differentially expressed genes induced by electrical stimulation, with 112 up-regulated
79 and 12 down-regulated **(Fig. 1c**; FDR<0.05, log2fold change>0.2; **Supplementary**
80 **Table 2).** Among the up-regulated genes, we observed induced expression of *NPAS4*,
81 *FOS*, and *NR4A1*, as well as cytokine-related genes *CCL3, CCL4, OSM,* and *RGS1.*
82 Notably, these genes were not significantly enriched for previously identified genes
83 induced in regions showing seizure activity in the human brain **(Extended Data Fig. 2)**
84 [14]. Enrichment network analysis was used to identify the pathways most represented
85 among the 124 differentially expressed genes in the stimulation paradigm. The
86 pathways include transcription at RNA polymerase II promoter, positive regulation of
87 DNA-dependent transcription, cytokine activity, chemokine activity, and cytokine
88 receptor binding **(Extended Data Fig. 3)**. Additional protein-protein interaction (PPI)
89 analysis of the stimulated samples revealed two significant clusters enriched with genes
90 involved in DNA-binding transcription activator activity (RNA Pol II) and cytokine activity
91 **(Fig. 1d)**. RNA-seq analysis comparing unstimulated samples with baseline identified
92 differential expression of only 16 genes, with 9 up-regulated and 7 down-regulated

genes; only NR4A3 overlapped between stimulated and unstimulated groups **(Fig. 1e, Supplementary Table 3).** The lack of extensive overlap between the differentially expressed genes observed in our unstimulated and stimulated groups suggests that the selective changes in gene expression that we see following electrical stimulation do not reflect disease state or surgical conditions such as craniotomy, brain temperature, and anesthesia, but reflect stimulation-induced changes. To investigate if these gene expression changes are unique to human samples and to further determine if they are related to disease state[14,15], we used a similar electrical stimulation paradigm in mouse non-primary auditory cortex and observed the upregulation of genes associated with DNA-binding transcription factor activity (*Fos*, *Fosb*, and *Egr2*) and cytokine activity (*Ccl3* and *Ccl4*) (**Extended Data Fig. 4**). Thus, our findings of activity-dependent genes in response to electrical stimulation in the human brain reveal a molecular signature that is conserved across species.

Next, we investigated the cell types exhibiting differential gene expression following electrical stimulation in the human brain by single nuclei multiomics (RNA and ATAC) on samples from the stimulated paradigm (**Fig 2a**). We sequenced 18,342 nuclei and detected 46,849 unique molecular identifiers and 2,133 median genes per nucleus (**Extended Data Fig. 5a**). Cell clustering analysis identified 7 major cell types in our samples (**Fig. 2b, c**). Importantly, the distribution and proportion of cell types was consistent across baseline and stimulated conditions (**Extended Data Fig. 5b**). We identified differentially expressed genes following electrical stimulation for the following cell types—excitatory neurons, microglia, vip-Sncg-Lamp5 inhibitory neurons, pvalb-Sst

116 inhibitory neurons, oligodendrocytes, oligodendrocytes precursor cells (OPC), and
117 astrocytes (**Fig. 2d-f, Supplementary Table 4**). Microglia displayed the highest
118 differential gene expression of all cell types with 306 up- and 296 down-regulated genes
119 (**Fig. 2d**). Genes related to cytokine activity (*CCL3*, *CCL4*, *IL1B*, *CCL2*, *IL1A*, *OSM* and
120 *RGS1*) were upregulated exclusively within microglia (**Fig. 2e; Extended Data Fig. 6a**).
121 In contrast, genes related to DNA-binding transcription activity (*FOS*, *EGR1*, *JUNB,* and
122 *EGR3*) were upregulated in neurons and microglia, whereas *NPAS4* and *EGR4* were
123 exclusively upregulated within excitatory and inhibitory neurons (**Fig. 2f, Extended Data**
124 **Fig. 6b**). Gene expression changes from microglia in the single nuclei multiomic
125 experiment significantly correlated with the bulk RNA-seq (**Fig. 2g, Extended Data Fig.**
126 **7-9)**. Interestingly, among the upregulated genes identified in bulk RNA-seq, we
127 discovered that 37 were upregulated in microglia. These results reveal that electrical
128 stimulation activates gene expression involved in transcriptional regulation in multiple
129 cell types and selectively activates genes involved in cytokine activity in microglia.
130
131 To investigate this cell-type-specific molecular signature further, we assessed chromatin
132 accessibility for activity-induced genes using single nuclear assay for transposase-
133 accessible chromatin with sequencing (snATAC-seq)[16] on human samples from the
134 stimulated paradigm. We found enriched promoter accessibility for 21 genes in
135 microglia that exhibited upregulated gene expression in the bulk RNA seq and
136 snRNAseq data (**Fig. 3a-b, Supplementary Table 5**), showing upregulation of
137 transcription factors *FOS*, *NR4A1*, *NR4A2*, and *NR4A3* and cytokine-related genes
138 *CCL4, CCL4L2* and *OSM.* Next, we performed transcription factor motif analysis using

139 the sn-ATAC seq data from microglia and found an enrichment of binding motifs for
140 SPIC, KLF6, SPI1, HOXB13, REL, and CREB1 (**Fig. 3c**). Notably, CREB, a master
141 regulator of activity-induced genes has been previously shown to be activated in
142 microglia[17]. pREL/NF-kB is a critical regulator of proinflammatory gene expression[18],
143 including genes encoding cytokines *IL1A* and *IL1B*, which were upregulated in our
144 snRNA-seq data (**Fig. 2d**). SPI1 is a central transcription factor essential for microglia
145 development and activation[19], and we found specific enrichment of SPI1 on the
146 promotor region for *CCL4* only in microglia, consistent with our snRNA-seq data (**Fig.**
147 **3d**). Within neuronal populations, the promoter region for *NPAS4* exhibited increased
148 accessibility in excitatory and inhibitory neurons in a region bound by CBP (**Fig. 3e**), a
149 transcriptional coactivator and lysine acetyltransferase that promotes the expression of
150 activity-induced genes[20]. Thus, our sn-ATAC-seq reveals a signature of transcription
151 factor motifs and chromatin accessibility to regulate activity-dependent gene expression
152 in specific cell types in response to electrical stimulation.
153
154 This work is the first to define activity-induced gene expression in the human brain,
155 revealing that electrical stimulation induces a distinct transcriptomic and epigenomic
156 signature in specific cell types in the human brain. Genes related to DNA-binding
157 transcription factor activity and cytokine signaling within microglia showed the greatest
158 induction pattern, and this was conserved across species. We observed the
159 hypothesized induction of the “classic” activity-dependent genes in neurons, but to our
160 surprise, our single nuclei multiomics experiments revealed pronounced microglia-
161 specific transcriptomic activation following electrical stimulation. The key observation of

162 an upregulation of the microglial response to electrical activation supports a paradigm
163 shift in interpreting the transcriptomic activation pattern following neural stimulation.
164 Microglia are critical modulators of neuronal activity, acting to suppress excessive
165 activity by inhibiting surrounding neurons, including excitatory neurons[21]. Researchers
166 have correlated human brain transcriptomics with prior recorded oscillatory signatures
167 of memory consolidation in human subjects [22,23], but this prior work did not identify
168 changes in gene expression driven by activity and they did not observe microglial-
169 specific changes. This identification of a microglial transcriptomic response following
170 electrical stimulation presents an important conceptual advance in our understanding of
171 activity-dependent gene expression in the human brain.
172
173 Our analyses identified critical molecular components that drive activity-dependent
174 changes in the function of brain circuits. Within neuronal cell types, the highest fold
175 change was observed for the *NPAS4*, which encodes a master transcriptional regulator
176 of learning-induced genes and is critical for memory consolidation[24]. Within microglia,
177 we identified the induction of cytokine-related genes including *CCL4*, which mediates
178 intracellular chemokine signaling, altering microglial process extension and motility,
179 influencing neuronal-microglial interactions, and shaping neuronal connectivity [21,25-27].
180 These mechanisms enable microglia to respond to neuronal activation and sculpt circuit
181 function. Our study of chromatin accessibility defines a cell-type-specific signature of
182 transcription factors driving these processes. Thus, our findings reveal distinct cell-type
183 specific mechanisms of activity-dependent changes in brain function, laying the

184 groundwork for future studies to link human brain transcription to closed-loop stimulation
185 and natural experience.
186
187 **Acknowledgments**
188 We thank Rashmi N. Mueller who oversaw anesthesia to manage pain levels before,
189 during, and after surgical procedures, and Kyle S. Conway for helping with initial
190 pathological assessment. We thank the Iowa Institute of Human Genetics (IIHG) core for
191 RNA seq library preparation and sequencing. We thank the Neural Circuits and Behavior
192 Core at the Iowa Neuroscience Institute for the use of their facilities. We thank the Iowa
193 NeuroBank Core for tissue collection and storage.
194 **Funding:** This work was supported by grants from the National Institute of Health R01
195 MH 087463 to T.A., The Gary & LaDonna Wicklund Research Fund for Cognitive Memory
196 Disorders to T.A., and The University of Iowa Hawkeye Intellectual and Developmental
197 Disabilities Research Center (HAWK-IDDRC) P50 HD103556 to T.A., The National
198 Institute of Health K99/R00 AG068306 to S.C., The National Institute of Health R01
199 DC004290 to M.A.H., T.A. is supported by the Roy J. Carver chair of neuroscience, T.N.J
200 & C.I.P. are supported a Research Program of Excellence of the Carver Trust. T.N.J.
201 was supported by the Andrew H. Woods Professorship.
202 **Author contributions:**
203 S.C., M.A.H. and T.A. conceived the project, designed the experiments, and interpreted
204 the data and wrote the manuscript with inputs from all the authors. H.K. performed human
205 surgery, electrical stimulation, and resected the tissue. A.E.R .and C.K.K. processed with
206 IRB and MRI imaging registration. H.O, M.A.H, T.N-J, K.V.L provided advise on surgical

procedure and electrical stimulation. M.M.H provided pathological assessment. L.C.L., K.V.N., and B.J.P. collected the tissue and images during resection. B.J.P., S.C. and L.C.L. generated the bulk RNA, single nuclei multiomics (RNA+ATAC) data. Y.V. performed the bioinformatics analysis with inputs from E.B. and J.J.M. S.A.H. performed the mouse surgery and electrical stimulation experiments. K.V.N, C.K.K, Z.K. Y.K, C.I.P, M.H, J.J.M, E.B, U.M, and T.N.J. provided input on data analysis and interpretation. C.I.P. and L.L. helped with manuscript writing. All authors discussed the results and commented on the manuscript.

Competing interests

T.A. is a scientific advisor to Aditum Bio and Radius Health and he serves on the scientific advisory board of Embark Neuro. T.A serves on the Scientific Advisory Board of EmbarkNeuro and is a scientific advisor to Aditum Bio and Radius Health. The other authors declare no conflicting interests.

Figure legends

Figure 1. **Stimulation alone induces gene expression changes in cytokine activity and DNA-binding transcription factor activity**. **a,b**. Schematics of stimulated (**a**) and unstimulated (**b**) paradigms in the human anterior temporal lobe. For both paradigms sample A was taken at T = 0 minutes then an adjacent sample B was taken at either T = 30 minutes after stimulation (**a**, stimulated paradigm, n=4 subjects) or T = 30 minutes after sample A was taken (**b**, unstimulated paradigm, n=4 subjects). **c.** Volcano plots showing gene expression changes in the stimulated paradigm. The most significant

genes (FDR < 0.05) are labeled in red (upregulated) or in blue (downregulated). **d.** STRING network of significantly affected genes from the stimulated paradigm showing a cytokine activity network in teal and a DNA-binding transcription factor activity network in green. The gene labels are colored based on the directionality of gene expression changes (blue = downregulated, red = upregulated). **e**. Volcano plots showing gene expression changes in the unstimulated paradigm. The most significant genes (FDR < 0.05) are labeled in red (upregulated) or in blue (downregulated).

Figure 2. Cell-type specific gene expression changes following electrical stimulation in human brain. a-c. Our multiomic approach (**a**) leads to the identification of specific cell-types (**b**) validated by the expression of specific biomarkers (**c**) using the RNA part of the assay. **d**. Heat map showing cell type specific expression of genes that were found to be differentially expressed in the bulk RNA seq. The fold-change of each gene is represented from blue (down-regulated) to red (up-regulated). **e,f.** Violin plots showing gene expression changes of CCL3, CCL4, NPAS4 and EGR4 in each cell-type for baseline (blue) and stimulated (red) conditions. A gene is either significantly upregulated (FDR number in red above the plot) or not significant (N.S. above the plot). **g**. Quadrant plot comparing gene expression changes (log10(FDR)*log2fold-change) between our bulk RNA-seq experiment (x-axis) and our multiomic snRNA-seq (y-axis) after stimulation. Genes in red in the top-right corner of the plot are significantly upregulated in both experiments. FDR thresholds of 0.05 are represented by dotted lines. The dashed line represents the linear regression applied to this quadrant plot. The R-squared value and its Pearson score statistic of the linear regression is displayed in

252 the top right corner of the plot. The doted lines represent the FDR < 0.05 threshold.
253 Most significant genes affected are labeled.
254 **Figure 3**. **Differential transcription start site accessibility correlates with gene**
255 **expression changes after simulation**. **a**. Volcano plot showing differential transcription
256 start site accessibility in microglia after stimulation. A gene is labeled if its gene
257 expression and transcription start site accessibility are significantly increased after
258 stimulation in both bulk RNA-seq and snATAC-seq respectively. **b**. Quadrant plot
259 comparing changes (log10(FDR)*log2fold-change) between gene expression of the
260 RNA assay (x-axis) and transcription start site accessibility (y-axis) in the microglia
261 cluster after stimulation. Genes in red in the top-right corner of the plot are significantly
262 upregulated in both experiments. FDR thresholds of 0.05 are represented by dotted
263 lines. The dashed line represents the linear regression applied to this quadrant plot. The
264 R-squared value and its Pearson score statistic of the linear regression is displayed in
265 the top right corner of the plot. The doted lines represent the FDR < 0.05 threshold.
266 Most significant genes affected are labeled. **c**. DNA motifs that are overrepresented in a
267 set of peaks that are differentially accessible in microglia after stimulation. Motifs are
268 ranked based on significance from the most significant left to right. **d-e**. Coverage plot
269 for CCL4 **(d)** and NPAS4 **(e)** from our multiomic experiment. Each track represents
270 normalized chromatin accessibility signal from the ATAC assay for each cell-type and
271 each condition (baseline or stimulated). At the end of each track there is a violin plot
272 showing gene expression changes of the gene from the RNA assay (**** = FDR <
273 0.0001). Chip-seq datasets of SPI1 from Human Fujioka acute myeloid leukaemia cells
274 [28] and CBP from human macrophages [29] are represented in the bigwig track. Genome

275 annotation is represented under the “Genes” track with blue rectangles representing
276 exons and an arrow showing the direction of transcription. Individual peak computed
277 from the peak calling is represented under the “Peak” by a grey rectangle. Each peak
278 that may regulate the gene is linked to its transcription start site by blue arcs under the
279 “Links” track. Genomic location and scale are located at the bottom of the plot.
280

281 **Materials and Methods:**

282 ***Subjects:*** The study subjects were 8 adult neurosurgical patients (6 female, 2 male, age
283 19-63 years old, median age 41 years old) with medically refractory epilepsy. The patients
284 were undergoing surgical resection of seizure foci following non-invasive video
285 electroencephalography (EEG) or invasive iEEG monitoring. All subjects were diagnosed
286 with intractable epilepsy. Additionally, Subject L472 had a cavernoma and Subject L475
287 had a dysembryoplastic neuroepithelial tumor. All subjects except #6 were non-smokers.
288 Subjects’ age, sex, surgery, and awake or sedative information were recorded (**Extended**
289 **Data Table 1)**. All subjects were native English speakers, 7 were right-handed, 1 was left-
290 handed, and all had left language dominance as determined by Wada tests. All subjects
291 underwent audiometric evaluation before the study, and none were found to have hearing
292 deficits or word recognition scores deemed sufficient to affect the findings presented in
293 this study. The vision was self-reported as normal or corrected to normal with glasses or
294 contact lenses. As determined by standard neuropsychological assessments, cognitive
295 function was in the average range in all subjects. Research protocols were approved by
296 the University of Iowa Institutional Review Board (IRB 201910791, 201911084) and the
297 National Institutes of Health, and written informed consent was obtained from all subjects.

298 ***Procedure:*** Surgery was performed under general anesthesia or monitored anesthetic
299 care. Standard craniotomy was performed by the same senior epilepsy surgeon in all
300 patients to reach the epilepsy focus, which involved the anterior and medial temporal lobe
301 in all patients except one who had a temporal encephalocele and surrounding
302 anterolateral temporal cortical focus. Cortical tissue from the anterior temporal lobe was
303 sampled for analysis. The experimental condition was defined by an electrical "stimulation
304 paradigm" and a control "no-stimulation paradigm**"**. The location of the sampled tissue is
305 plotted on anatomic brain reconstructions **(Extended data fig 1).** All subjects underwent
306 resection surgery for epilepsy of various etiologies **(Extended data fig 1).** There were 4
307 subjects (1 iEEG and 3 EEG patients) who underwent the "stimulation paradigm" and 4
308 subjects (2 iEEG and 2 EEG patients) who underwent the "no-stimulation paradigm"
309 **(Extended Data Table 5)**.
310 In the "stimulation paradigm", a baseline sample was obtained from the anterior temporal
311 cortex that would be included in the planned surgical resection. The area directly adjacent
312 to where the baseline sample was collected was stimulated with direct bipolar electric
313 stimulation (frequency 50 Hz, pulse duration of 0.2 ms, stimulation duration 2 min, voltage
314 10 V, a commonly used stimulation parameters for deep brain stimulation for example).
315 The stimulated area was then sampled after a period of 30 minutes to allow for gene
316 expression[30,31]. In the "no stimulation paradigm", no direct electric stimulation was
317 performed and the area directly adjacent to the baseline sample was collected 30 minutes
318 after initial baseline sampling.
319 After sampling they were immediately placed in a sterile container on dry ice. The average
320 weight of the baseline sample was 88.0 ± 33.2 mg (mean, standard deviation) and the

321 adjacent sample was 113.4 ± 62.7 mg. After the collection of all samples in this fashion,
322 they were weighed and transferred to a freezer at -80° C for storage until further testing.
323 ***Sample Localization to MNI space:*** All samples were from the same cortical region.
324 Intraoperative photos of the sample sites were obtained during the time of surgery. Using
325 subject matched preoperative T1 sequence MRI, the sample sites were mapped onto
326 their anatomic brain reconstructions **(Extended data fig. 1)**. They were also mapped onto
327 MNI space coordinates.
328 ***RNA extraction, library preparation, and sequencing:*** Total RNA was extracted from
329 sampled human brains_using miRNeasy Mini Kit (Qiagen, CA, USA). The tissue
330 samples were homogenized in QIAzol (Qiagen, CA. USA) stainless steel beads
331 (Qiagen, CA, USA). Chloroform was then used for phase separation. RNA containing
332 an aqueous layer was further purified using the RNeasy MinElute spin column. RNA
333 was finally eluted in RNase-free water. RNA concentrations were estimated using a
334 Nanodrop (Thermo Fisher Scientific, MA, USA) and Qubit (Thermo Fisher Scientific,
335 MA, USA). RNA libraries were prepared at the Iowa Institute of Human Genetics (IIHG),
336 Genomics Division, using the Illumina Stranded Total RNA Prep, Ligation with Ribo-Zero
337 Plus (Illumina Inc., San Diego, CA). The KAPA Illumina Library Quantification Kit (KAPA
338 Biosystems, Wilmington, MA) was used to measure library concentrations. Pooled
339 libraries were sequenced on Illumina NovaSeq6000 sequencers with 150-bp paired-end
340 chemistry (Illumina) at the Iowa Institute of Human Genetics (IIHG) core.
341 ***Bulk RNA sequencing analysis:*** RNA-seq data were processed with the bcbio-nextgen
342 pipeline (https://github.com/bcbio/bcbio-nextgen, version 1.2.9). The pipeline uses
343 STAR[32] to align reads to the hg38 genome build (GENCODE release M10, Ensembl 89

344 annotation) and quantifies expression at the gene level with featureCounts [33]. All further
345 analyses were performed using R. For gene-level count data, the R package EDASeq
346 was used to account for sequencing depth (upper quartile normalization)[34]. Latent
347 sources of variation in expression levels were assessed and accounted for using RUVSeq
348 (RUVs mode using all features)[35]. Appropriate choice of the RUVSeq parameter k was
349 guided through inspection of principal components analysis (PCA) plots. Specifically, the
350 smallest value k was chosen where PCA plots demonstrated replicate sample clustering
351 in the first three principal components[36]. Differential expression analysis was conducted
352 using the edgeR package[37]. Codes to reproduce the RNA-seq differential gene
353 expression analysis are available at https://github.com/YannVRB/Human-brain-
354 stimulation.git.
355 All the transcriptomics data have been deposited in NCBI's Gene Expression Omnibus
356 and are accessible through GEO Series accession number GSE224952.
357 ***Downstream pathway analysis:*** Enrichment analysis of differentially expressed genes-
358 associated pathways and molecular functions from the stimulated and unstimulated RNA-
359 seq was performed with the Gene Ontology (GO–molecular function) databases. Only the
360 pathways with an adjusted p-value < 0.05 were considered as significant and displayed.
361 Data were visualized using NetworkAnalyst (www.networkanalyst.ca). The protein-protein
362 interactive network was constructed using STRING (version 11.5), which uses the
363 STRING database (http://string-db.org/). The PPI network was constructed to identify the
364 interactions between proteins encoded by differentially expressed genes (FDR<0.05)
365 based on experimental data. The differentially expressed genes names were pasted into
366 the "STRING protein query." Active interaction sources, including text mining,

367 experiments, databases, coexpression, neighborhood, gene fusion, and co-occurrence,
368 were applied, and high interaction score confidence (0.700) was selected to construct the
369 PPI network. Full network was constructed, where the edges indicate both functional and
370 physical protein associations. The network edges were constructed based on evidence,
371 where line color indicates the type of interaction evidence.

372 ***Single-nuclei multiomics (nuclei isolation, library preparation, sequencing):*** Nuclei
373 were isolated from brain tissue using the Chromium Nuclei Isolation Kit (10X Genomics).
374 Briefly, frozen tissue was dissociated with pestle in lysis buffer, passed through nuclei
375 isolation column and spun at 16,000 rcf for 20 sec at 4^0C. Flowthrough was vortexed and
376 spun at 500 rcf for 3 mins at 4^0C. Pellet was resuspended with debris removal buffer and
377 centrifuged at 700 rcf for 10 mins at 4^0C, nuclei resuspended in wash buffer and
378 centrifuged again at 500 rcf for 5 mins at 4^0C. Pellet was resuspended in resuspension
379 buffer and nuclei were counted using a hemocytometer. Nuclei were directly processed
380 for droplet capture for single cell multiome ATAC + gene expression using a chromium
381 controller (10X Genomics). Chromium Next GEM Single Cell Multiome ATAC + Gene v1
382 chemistry was used to create single nuclei ATAC and RNA libraries from the same cell.
383 Two baseline and two stimulated samples were used for independent replicates. Libraries
384 were sequenced on an Illumina Novaseq 6000 with a 150 bp paired end read setup.

385 ***Single-nuclei multiomic data processing and analysis:***

386 Raw sequencing data were processed using the Cell Ranger ARC pipeline (v2.0.2) with
387 the cellranger-arc mm10 reference. Default parameters were used to align reads, count
388 unique fragments or transcripts, and filter high-quality nuclei. Individual HDF5 files for
389 each sample containing RNA counts and ATAC fragments per cell barcode were loaded

390 into Seurat (Read10X_h5) resulting in four Seurat objects, each containing both RNA and
391 ATAC assays. Nuclei with outliers ATAC and RNA QC metrics (<1,000 and >100,000
392 ATAC read counts, <1,000 and >25,000 RNA read counts, nucleosomal signal > 2, TSS
393 enrichment < 1, and percentage of mitochondrial reads > 20) were removed. To correctly
394 identify cell type-specific signature, the RNA assay was chosen because it leads to less
395 background noise for the expression of biomarkers.
396 To analyze the RNA part of the human brain stimulation multiomic data, gene counts were
397 normalized and log transformed (LogNormalize), and the top 2,000 most variable features
398 between each nuclei were identified using FindVariableFeatures
399 (selection.method = 'vst'). Features that are repeatedly variable across nuclei and
400 datasets were selected for integration (SelectIntegrationFeatures). We then identified
401 anchors (FindIntegrationAnchors), which took the list of 4 individual Seurat objects for
402 each sample as input and used these anchors to integrate the four datasets together
403 (IntegrateData). The following analyses were performed on the integrated Seurat object.
404 Linear dimensionality reduction was performed by principal component analysis (runPCA,
405 npcs = 25). A k-nearest-neighbors graph was constructed based on Euclidean distance in
406 PCA space and refined (FindNeighbors, npcs = 30), then nuclei were clustered using the
407 Louvain algorithm (FindClusters, resolution = 0.5). Clusters were visualized with UMAP
408 (runUMAP, dims = 30). Cell types were annotated by label transfer cell labels from an
409 existing human primary motor cortex reference dataset from the Allen Institute (doi:
410 10.1038/s41586-021-03465-8) (FindTransferAnchors and TransferData). Cell types
411 identification was validated by expression of specific biomarkers (Fig. 2c). Differentially

412 expressed genes (DEGs) in individual clusters between baseline and stimulated samples
413 were calculated (FindMarkers, test.use = 'wilcox', Padj < 0.05, logfc.threshold > |0.2|).
414 To analyze ATAC part of the human brain stimulation multiomic data, prior to integrating
415 the four Seurat object, the default assay was switched to ATAC, and peak calling was
416 performed. Since the set of peaks identified by Cellranger often merges distinct peaks
417 that are close together, creating a problem for motif enrichment analysis and peak-to-
418 gene linkage, we identified a more accurate set of peaks by calling peaks using MACS2
419 (CallPeaks) on all cells together. Peaks on nonstandard chromosomes and in genomic
420 blacklist regions were removed (keepStandardChromosomes and subsetByOverlaps).
421 Normalization was performed with a frequency-inverse document frequency
422 normalization which normalizes across cells and peaks (RunTFIDF). Then, a feature
423 selection was performed using all the peaks as input (FindTopFeatures). The dimensional
424 reduction was performed on the TF-IDF normalized matrix with the selected peaks using
425 a singular value decomposition (RunSVD). To mimic the open chromatin conformation of
426 a gene, a gene activity matrix was calculated using a window of 1000bp before and after
427 the transcription start site of each protein coding gene (GeneActivity). Differentially
428 accessible transcription start sites in individual clusters between baseline and stimulated
429 samples were calculated using a logistic regression framework (FindMarkers, test.use =
430 'LR', latent.vars = 'nCount_peaks', Padj < 0.05). Motif and transcription factor enrichment
431 analysis of transcription start sites gene activity for each cluster was performed using
432 FindMotifs. The top six enriched motifs in microglia cluster are shown in **Figure. 3c**.
433 Genomic locations of typical genes like CCL4 and NPAS4 were presented (CoveragePlot)
434 and includes chip-seq datasets (bigwig) of SPI1 from Human Fujioka acute myeloid

435 leukaemia cells [28] and CBP from human macrophages [29]. It also includes co-accessibility
436 between peaks and transcription start site of genes. Codes to reproduce the multiomic
437 data analysis are available at https://github.com/YannVRB/Human-brain-stimulation.git.
438 ***Animals:*** Adult male C57BL/6J mice were purchased from The Jackson Laboratory were
439 3 to 4 months of age during experiments. All mice had free access to food and water;
440 lights were maintained on a 12-hour light/12-hour dark cycle.
441 ***Mouse electrical stimulation:*** Stimulation experiments were performed in anesthetized
442 adult male C57BL6/J mice. Anesthesia was induced with 5% isoflurane by inhalation
443 and maintained at 1.8-2% for the duration of the experiment. The mouse was placed in
444 a stereotax (Kopf) and a midline incision was made and the skin retracted to expose the
445 temporal muscle bilaterally. The dorsal insertion of both temporal muscles was
446 removed, and the muscles retracted. A 2-3 mm craniotomy was made over area AuV
447 (centered at 2.9 mm posterior, 4.2 mm lateral, 2.8 mm ventral from Bregma based on
448 Paxinos atlas) bilaterally to expose the cortical surface and a small square of gel foam
449 soaked in ACSF was applied on top of the dura to prevent it from dehydrating. For each
450 mouse the side of electrical stimulation and sham stimulation were alternated, with the
451 sham side serving as the baseline control for gene expression profiling. Electrical
452 stimulation was delivered through a bipolar ball electrode constructed from two silver
453 wires in which the uninsulated tips were melted under a butane flame (1 mm tip size, 2
454 mm tip spacing). For both electrical and sham stimulations, the gel foam was removed
455 and the electrode was gently lowered to make contact with the cortical surface. For
456 electrical stimulation, a biphasic pulse train was then delivered for two minutes (8 mA,
457 50 Hz, 200 μs pulse width). For the sham stimulation no current was delivered but the

458 electrode was left in place for 2 minutes. Following electrical or sham stimulation the
459 electrode was slowly retracted, and the exposed dura was covered with gel foam.
460 Selection for hemisphere was performed randomly, which resulted in the order of
461 electrical and sham stimulation alternating from mouse to mouse. No more than 5
462 minutes elapsed between electrical or sham stimulation of both sides. After both sides
463 were stimulated (electrical or sham) the mouse was left in the stereotax under
464 anesthesia for 30 minutes before euthanasia and tissue collection. Tissue samples were
465 immediately stored at -80^{0}C in RNA later solution (Ambion).
466 ***RNA extraction, cDNA preparation and qPCRs from mouse auditory cortex:*** Tissue
467 samples were homogenized in Qiazol (Qiagen) using stainless steel beads (Qiagen).
468 Chloroform was added and centrifuged at 12,000*g* at room temperature for 15 min to
469 separate RNA in the aqueous phase. RNA was precipitated in ethanol and cleared using
470 RNeasy kit (Qiagen). RNA eluted in nuclease-free water was then treated with DNase
471 (Qiagen) at room temperature for 25 min to remove genomic DNA. RNA was further
472 precipitated in ethanol, sodium acetate (pH 5.2) and glycogen overnight at −20°C. RNA
473 was precipitated by centrifugation at 30,000g for 20 min, precipitate washed with 70%
474 ethanol and the dried RNA pellet was resuspended in nuclease-free water. RNA
475 concentration was measured using NanoDrop (Thermo Fisher Scientific). 1 µg of RNA
476 was used for complementary DNA (cDNA) preparation using the SuperScript IV First-
477 Strand Synthesis System (Ambion). Real-time reverse transcription polymerase chain
478 reactions (RT-PCRs) were performed on the QuantStudio 7 Flex Real-Time PCR System
479 (Applied Biosystems, Life Technologies). Data were normalized to housekeeping genes
480 (*Tubulin*, *Pgk1*, and *Actin*), and $2^{(-\Delta\Delta Ct)}$ method was used for gene expression analysis.

481 ***Statistics***: For the qPCR analysis, the Wilcoxon matched pairs signed rank test and one

482 sample Wilcoxon test was performed.

483

484 **References**

485 1 Yap, E. L. & Greenberg, M. E. Activity-Regulated Transcription: Bridging the Gap
486 between Neural Activity and Behavior. *Neuron* **100**, 330-348 (2018).
487 https://doi.org:10.1016/j.neuron.2018.10.013

488 2 Sagar, S. M., Sharp, F. R. & Curran, T. Expression of c-fos protein in brain:
489 metabolic mapping at the cellular level. *Science* **240**, 1328-1331 (1988).
490 https://doi.org:10.1126/science.3131879

491 3 Guzowski, J. F., McNaughton, B. L., Barnes, C. A. & Worley, P. F. Environment-
492 specific expression of the immediate-early gene Arc in hippocampal neuronal
493 ensembles. *Nat Neurosci* **2**, 1120-1124 (1999). https://doi.org:10.1038/16046

494 4 Laricchiuta, D. *et al.* Optogenetic Stimulation of Prelimbic Pyramidal Neurons
495 Maintains Fear Memories and Modulates Amygdala Pyramidal Neuron
496 Transcriptome. *Int J Mol Sci* **22** (2021). https://doi.org:10.3390/ijms22020810

497 5 Bali, P. & Kenny, P. J. Transcriptional mechanisms of drug addiction. *Dialogues*
498 *Clin Neurosci* **21**, 379-387 (2019).
499 https://doi.org:10.31887/DCNS.2019.21.4/pkenny

500 6 Fernandez-Albert, J. *et al.* Immediate and deferred epigenomic signatures of in
501 vivo neuronal activation in mouse hippocampus. *Nat Neurosci* **22**, 1718-1730
502 (2019). https://doi.org:10.1038/s41593-019-0476-2

503 7 Marco, A. *et al.* Mapping the epigenomic and transcriptomic interplay during
504 memory formation and recall in the hippocampal engram ensemble. *Nat Neurosci*
505 **23**, 1606-1617 (2020). https://doi.org:10.1038/s41593-020-00717-0

506 8 Reijmers, L. G., Perkins, B. L., Matsuo, N. & Mayford, M. Localization of a stable
507 neural correlate of associative memory. *Science* **317**, 1230-1233 (2007).
508 https://doi.org:10.1126/science.1143839

509 9 Halder, R. *et al.* DNA methylation changes in plasticity genes accompany the
510 formation and maintenance of memory. *Nat Neurosci* **19**, 102-110 (2016).
511 https://doi.org:10.1038/nn.4194

512 10 Boulting, G. L. *et al.* Activity-dependent regulome of human GABAergic neurons
513 reveals new patterns of gene regulation and neurological disease heritability. *Nat*
514 *Neurosci* **24**, 437-448 (2021). https://doi.org:10.1038/s41593-020-00786-1

515 11 Inman, C. S. *et al.* Direct electrical stimulation of the amygdala enhances
516 declarative memory in humans. *Proc Natl Acad Sci U S A* **115**, 98-103 (2018).
517 https://doi.org:10.1073/pnas.1714058114

12 Ezzyat, Y. *et al.* Closed-loop stimulation of temporal cortex rescues functional networks and improves memory. *Nat Commun* **9**, 365 (2018). https://doi.org:10.1038/s41467-017-02753-0

13 Scangos, K. W., Makhoul, G. S., Sugrue, L. P., Chang, E. F. & Krystal, A. D. State-dependent responses to intracranial brain stimulation in a patient with depression. *Nat Med* **27**, 229-231 (2021). https://doi.org:10.1038/s41591-020-01175-8

14 Brueggeman, L. *et al.* Drug repositioning in epilepsy reveals novel antiseizure candidates. *Ann Clin Transl Neurol* **6**, 295-309 (2019). https://doi.org:10.1002/acn3.703

15 Altmann, A. *et al.* A systems-level analysis highlights microglial activation as a modifying factor in common epilepsies. *Neuropathol Appl Neurobiol* **48**, e12758 (2022). https://doi.org:10.1111/nan.12758

16 Morabito, S. *et al.* Single-nucleus chromatin accessibility and transcriptomic characterization of Alzheimer's disease. *Nat Genet* **53**, 1143-1155 (2021). https://doi.org:10.1038/s41588-021-00894-z

17 Gao, Y. *et al.* Microglia CREB-Phosphorylation Mediates Amyloid-beta-Induced Neuronal Toxicity. *J Alzheimers Dis* **66**, 333-345 (2018). https://doi.org:10.3233/JAD-180286

18 Tak, P. P. & Firestein, G. S. NF-kappaB: a key role in inflammatory diseases. *J Clin Invest* **107**, 7-11 (2001). https://doi.org:10.1172/JCI11830

19 Jones, R. E., Andrews, R., Holmans, P., Hill, M. & Taylor, P. R. Modest changes in Spi1 dosage reveal the potential for altered microglial function as seen in Alzheimer's disease. *Sci Rep* **11**, 14935 (2021). https://doi.org:10.1038/s41598-021-94324-z

20 Kim, T. K. *et al.* Widespread transcription at neuronal activity-regulated enhancers. *Nature* **465**, 182-187 (2010). https://doi.org:10.1038/nature09033

21 Badimon, A. *et al.* Negative feedback control of neuronal activity by microglia. *Nature* **586**, 417-423 (2020). https://doi.org:10.1038/s41586-020-2777-8

22 Berto, S. *et al.* Gene-expression correlates of the oscillatory signatures supporting human episodic memory encoding. *Nat Neurosci* **24**, 554-564 (2021). https://doi.org:10.1038/s41593-021-00803-x

23 Berto, S., Wang, G. Z., Germi, J., Lega, B. C. & Konopka, G. Human Genomic Signatures of Brain Oscillations During Memory Encoding. *Cereb Cortex* **28**, 1733-1748 (2018). https://doi.org:10.1093/cercor/bhx083

24 Ramamoorthi, K. *et al.* Npas4 regulates a transcriptional program in CA3 required for contextual memory formation. *Science* **334**, 1669-1675 (2011). https://doi.org:10.1126/science.1208049

25 Liu, Y. U. *et al.* Neuronal network activity controls microglial process surveillance in awake mice via norepinephrine signaling. *Nat Neurosci* **22**, 1771-1781 (2019). https://doi.org:10.1038/s41593-019-0511-3

26 Stowell, R. D. *et al.* Noradrenergic signaling in the wakeful state inhibits microglial surveillance and synaptic plasticity in the mouse visual cortex. *Nat Neurosci* **22**, 1782-1792 (2019). https://doi.org:10.1038/s41593-019-0514-0

27 Cheadle, L. *et al.* Sensory Experience Engages Microglia to Shape Neural Connectivity through a Non-Phagocytic Mechanism. *Neuron* **108**, 451-468 e459 (2020). https://doi.org:10.1016/j.neuron.2020.08.002

28 Simeoni, F. *et al.* Enhancer recruitment of transcription repressors RUNX1 and TLE3 by mis-expressed FOXC1 blocks differentiation in acute myeloid leukemia. *Cell Rep* **36**, 109725 (2021). https://doi.org:10.1016/j.celrep.2021.109725

29 Kang, K. *et al.* IFN-gamma selectively suppresses a subset of TLR4-activated genes and enhancers to potentiate macrophage activation. *Nat Commun* **10**, 3320 (2019). https://doi.org:10.1038/s41467-019-11147-3

30 Hansson, A. C. & Fuxe, K. Time-course of immediate early gene expression in hippocampal subregions of adrenalectomized rats after acute corticosterone challenge. *Brain Res* **1215**, 1-10 (2008). https://doi.org:10.1016/j.brainres.2008.03.080

31 Cullinan, W. E., Herman, J. P., Battaglia, D. F., Akil, H. & Watson, S. J. Pattern and time course of immediate early gene expression in rat brain following acute stress. *Neuroscience* **64**, 477-505 (1995). https://doi.org:10.1016/0306-4522(94)00355-9

32 Dobin, A. *et al.* STAR: ultrafast universal RNA-seq aligner. *Bioinformatics* **29**, 15-21 (2013). https://doi.org:10.1093/bioinformatics/bts635

33 Liao, Y., Smyth, G. K. & Shi, W. featureCounts: an efficient general purpose program for assigning sequence reads to genomic features. *Bioinformatics* **30**, 923-930 (2014). https://doi.org:10.1093/bioinformatics/btt656

34 Risso, D., Schwartz, K., Sherlock, G. & Dudoit, S. GC-content normalization for RNA-Seq data. *BMC Bioinformatics* **12**, 480 (2011). https://doi.org:10.1186/1471-2105-12-480

35 Risso, D., Ngai, J., Speed, T. P. & Dudoit, S. Normalization of RNA-seq data using factor analysis of control genes or samples. *Nat Biotechnol* **32**, 896-902 (2014). https://doi.org:10.1038/nbt.2931

36 Peixoto, L. *et al.* How data analysis affects power, reproducibility and biological insight of RNA-seq studies in complex datasets. *Nucleic Acids Res* **43**, 7664-7674 (2015). https://doi.org:10.1093/nar/gkv736

37 Robinson, M. D., McCarthy, D. J. & Smyth, G. K. edgeR: a Bioconductor package for differential expression analysis of digital gene expression data. *Bioinformatics* **26**, 139-140 (2010). https://doi.org:10.1093/bioinformatics/btp616

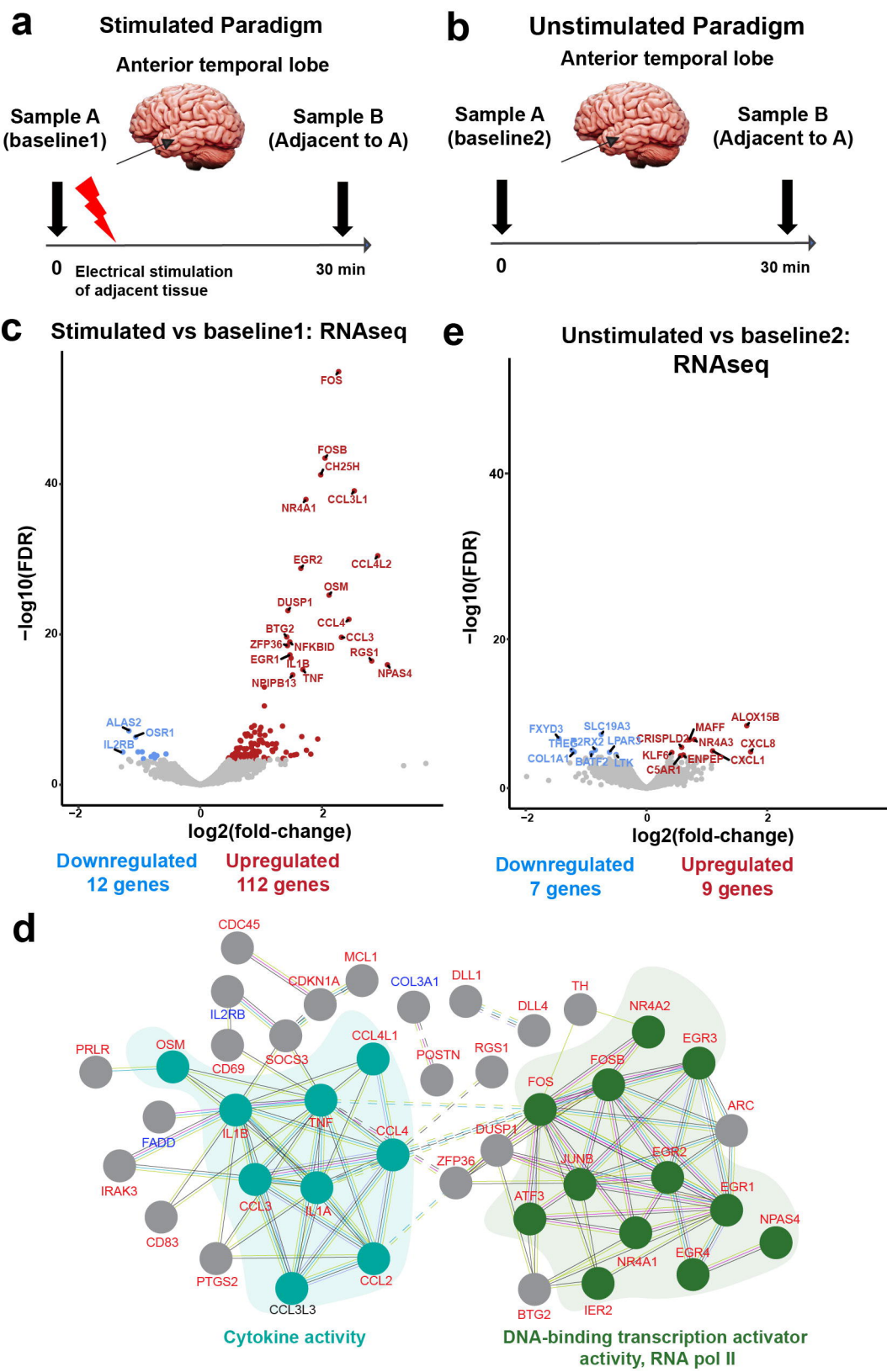
a
Stimulated Paradigm
Anterior temporal lobe
Sample A (baseline1)
Sample B (Adjacent to A)
0
Electrical stimulation of adjacent tissue
30 min
b
Unstimulated Paradigm
Anterior temporal lobe
Sample A (baseline2)
Sample B (Adjacent to A)
0
30 min
c
Stimulated vs baseline1: RNAseq
−log10(FDR)
log2(fold-change)
FOS
FOSB
CH25H
CCL3L1
NR4A1
EGR2
CCL4L2
OSM
DUSP1
CCL4
BTG2
CCL3
ZFP36
NFKBID
RGS1
EGR1
IL1B
NPAS4
TNF
NBIPB13
ALAS2
OSR1
IL2RB
Downregulated 12 genes
Upregulated 112 genes
e
Unstimulated vs baseline2: RNAseq
−log10(FDR)
log2(fold-change)
ALOX15B
MAFF
FXYD3
SLC19A3
CRISPLD2
NR4A3
CXCL8
THEM
P2RX2
LPAR3
COL1A1
BATF2
LTK
KLF6
ENPEP
CXCL1
C5AR1
Downregulated 7 genes
Upregulated 9 genes
d
CDC45
MCL1
CDKN1A
COL3A1
DLL1
TH
DLL4
NR4A2
IL2RB
PRLR
OSM
CD69
SOCS3
CCL4L1
POSTN
RGS1
EGR3
FOSB
FOS
ARC
FADD
IL1B
TNF
CCL4
DUSP1
ZFP36
JUNB
EGR2
IRAK3
CCL3
IL1A
ATF3
EGR1
NPAS4
CD83
NR4A1
EGR4
PTGS2
CCL2
CCL3L3
BTG2
IER2
Cytokine activity
DNA-binding transcription activator activity, RNA pol II

Figure 1

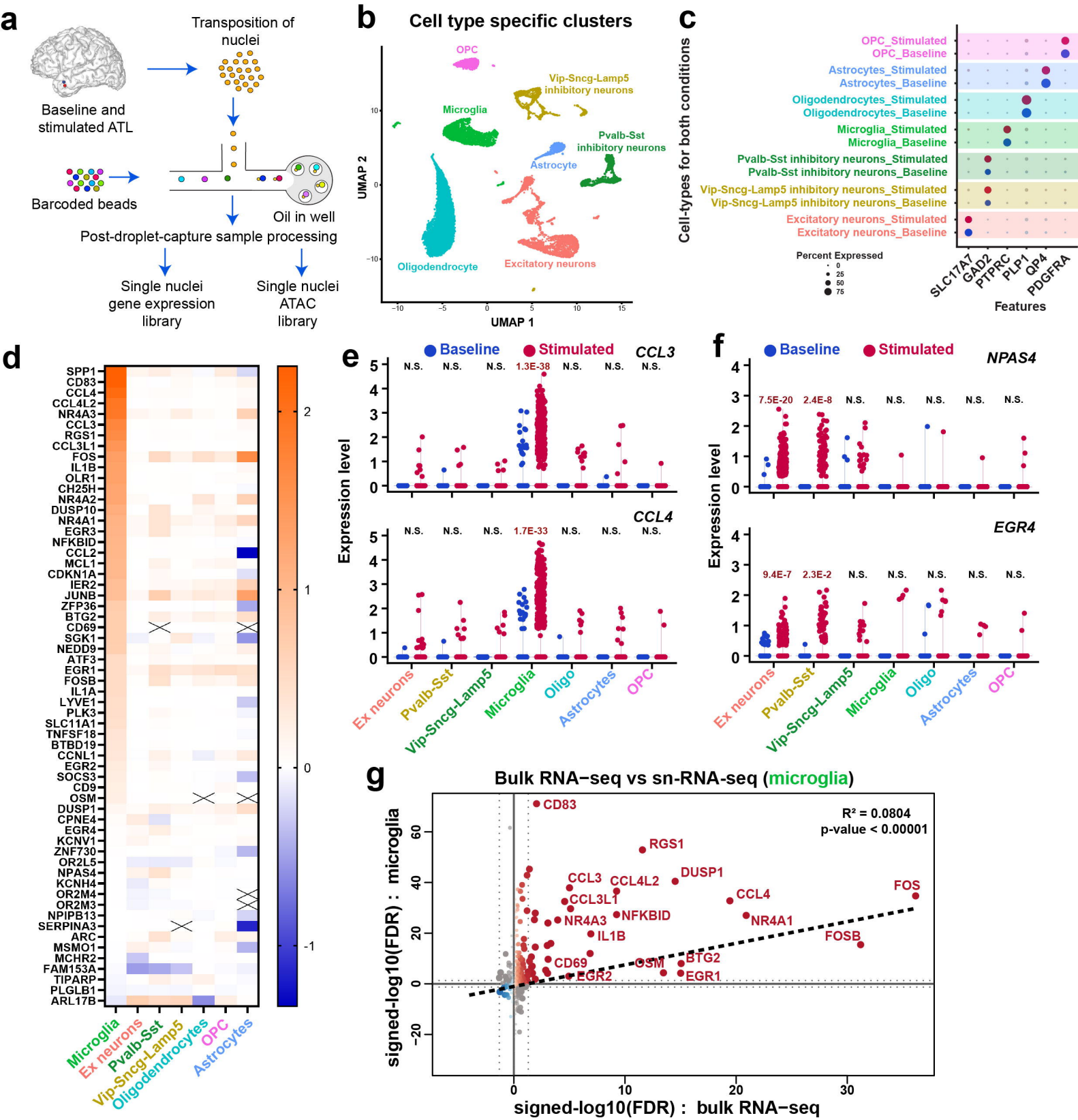
a
Transposition of nuclei
Baseline and stimulated ATL
Barcoded beads
Oil in well
Post-droplet-capture sample processing
Single nuclei gene expression library
Single nuclei ATAC library
b
Cell type specific clusters
OPC
Vip-Sncg-Lamp5 inhibitory neurons
Microglia
Pvalb-Sst inhibitory neurons
Astrocyte
Oligodendrocyte
Excitatory neurons
UMAP 1
UMAP 2
c
Cell-types for both conditions
OPC_Stimulated
OPC_Baseline
Astrocytes_Stimulated
Astrocytes_Baseline
Oligodendrocytes_Stimulated
Oligodendrocytes_Baseline
Microglia_Stimulated
Microglia_Baseline
Pvalb-Sst inhibitory neurons_Stimulated
Pvalb-Sst inhibitory neurons_Baseline
Vip-Sncg-Lamp5 inhibitory neurons_Stimulated
Vip-Sncg-Lamp5 inhibitory neurons_Baseline
Excitatory neurons_Stimulated
Excitatory neurons_Baseline
Percent Expressed
SLC17A7
GAD2
PTPRC
PLP1
QP4
PDGFRA
Features
d
Microglia
Ex neurons
Pvalb-Sst
Vip-Sncg-Lamp5
Oligodendrocytes
OPC
Astrocytes
e
Baseline
Stimulated
CCL3
CCL4
Expression level
Ex neurons
Pvalb-Sst
Vip-Sncg-Lamp5
Microglia
Oligo
Astrocytes
OPC
f
NPAS4
EGR4
7.5E-20
2.4E-8
9.4E-7
2.3E-2
g
Bulk RNA−seq vs sn-RNA-seq (microglia)
R² = 0.0804
p-value < 0.00001
signed-log10(FDR) : microglia
signed-log10(FDR) : bulk RNA−seq

Figure 2

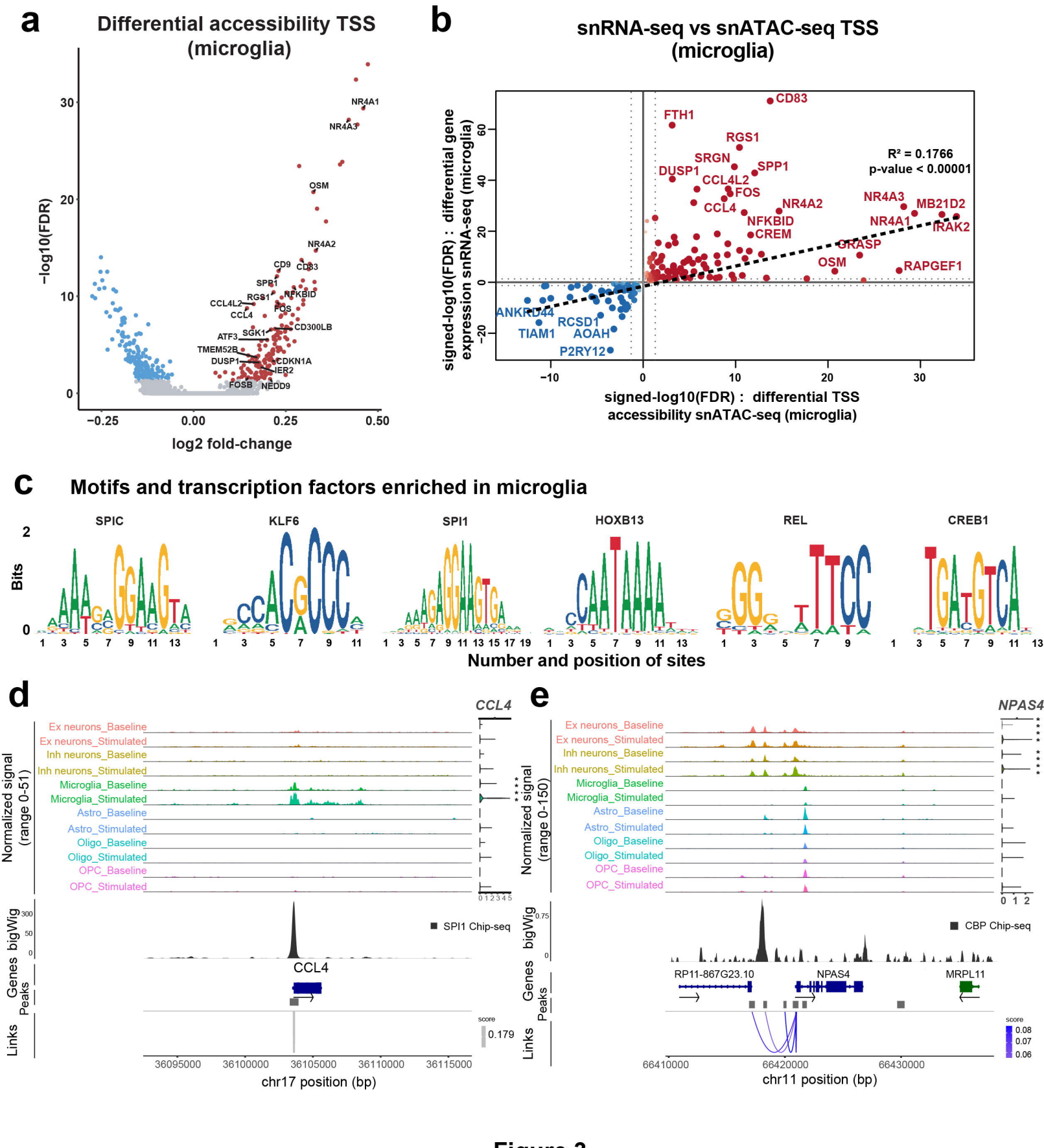
a
Differential accessibility TSS (microglia)
−log10(FDR)
log2 fold-change
NR4A1
NR4A3
OSM
NR4A2
CD9
CD83
SPP1
RGS1
NFKBID
CCL4L2
FOS
CCL4
CD300LB
SGK1
ATF3
TMEM52B
DUSP1
CDKN1A
IER2
FOSB
NEDD9
b
snRNA-seq vs snATAC-seq TSS (microglia)
signed-log10(FDR) : differential gene expression snRNA-seq (microglia)
signed-log10(FDR) : differential TSS accessibility snATAC-seq (microglia)
R² = 0.1766
p-value < 0.00001
CD83
FTH1
RGS1
SRGN
SPP1
DUSP1
CCL4L2
FOS
CCL4
NR4A2
NFKBID
CREM
NR4A3
MB21D2
NR4A1
IRAK2
GRASP
OSM
RAPGEF1
ANKRD44
RCSD1
TIAM1
AOAH
P2RY12
c
Motifs and transcription factors enriched in microglia
SPIC
KLF6
SPI1
HOXB13
REL
CREB1
Bits
Number and position of sites
d
CCL4
Normalized signal (range 0-51)
Ex neurons_Baseline
Ex neurons_Stimulated
Inh neurons_Baseline
Inh neurons_Stimulated
Microglia_Baseline
Microglia_Stimulated
Astro_Baseline
Astro_Stimulated
Oligo_Baseline
Oligo_Stimulated
OPC_Baseline
OPC_Stimulated
bigWig
SPI1 Chip-seq
Genes
Peaks
Links
score
0.179
36095000
36100000
36105000
36110000
36115000
chr17 position (bp)
e
NPAS4
Normalized signal (range 0-150)
CBP Chip-seq
RP11-867G23.10
NPAS4
MRPL11
score
0.08
0.07
0.06
66410000
66420000
66430000
chr11 position (bp)

Figure 3